N96-10447

Modeling Ka-band Low Elevation Angle Propagation Statistics

Thomas A. Russell, John Weinfield, Chris Pearson, and Louis J. Ippolito
Stanford Telecom
1761 Business Center Drive
Reston, VA 22090

Abstract

The statistical variability of the secondary atmospheric propagation effects on satellite communications cannot be ignored at frequencies of 20 GHz or higher, particularly if the propagation margin allocation is such that link availability falls below 99%. The secondary effects considered in this paper are gaseous absorption, cloud absorption, and tropospheric scintillation; rain attenuation is the primary effect. Techniques and example results are presented for estimation of the overall combined impact of the atmosphere on satellite communications reliability. Statistical methods are employed throughout and the most widely accepted models for the individual effects are used wherever possible. The degree of correlation between the effects is addressed and some bounds on the expected variability in the combined effects statistics are derived from the expected variability in correlation. Example estimates are presented of combined effects statistics in the Washington D.C. area at 20 GHz and 5° elevation angle. The statistics of water vapor are shown to be sufficient for estimation of the statistics of gaseous absorption at 20 GHz. A computer model based on monthly surface weather is described and tested. Significant improvement in prediction of absorption extremes is demonstrated with the use of path weather data instead of surface data.

I. Introduction

Traditionally, the allocation of power margin for propagation effects in a satellite communications link budget requires a statistical distribution of rain attenuation based on climatic region together with a fixed estimate of gaseous absorption derived from the mean temperature and humidity at the ground. The absorption level is subtracted from the link budget, and the statistics of link reliability are mapped directly from the statistics of rain attenuation. In the Ka band (30 GHz uplink / 20 GHz downlink) and above, however, fluctuations over the course of the year in gaseous absorption, cloud absorption, and tropospheric scintillation produce strong fades that often may occur simultaneously. Since rain attenuation is also higher at Ka band, the impact of these secondary effects (where rain attenuation remains the primary effect) depends on the level of total available propagation margin and the corresponding expected link availability.

The high levels of link availability (99.5% or higher) achievable at lower frequencies are very expensive to maintain at Ka band in light of the strong rain attenuation. Hence, lower availability levels (99% and less) are often accepted, corresponding to low rain rates (often 3 mm/hr and less), where the secondary effects become more pronounced relative to the rain attenuation. Such systems are referred to as low fade margin or low availability systems. For these systems, the statistical variability of the secondary effects should be combined with the statistics of rain attenuation in a way that incorporates the expected

correlations, in order to produce legitimate and useful estimates of the expected link availability. Similar assertions are made in [1-3]. In addition, significant work has been produced by the Helsinki University of Technology on many aspects of this topic [4-7].

Figure 1 presents an example of the relative fades produced by the three relatively slow-fading effects, fades which could at times produce a total attenuation equal to the sum of the individual fade levels. Scintillation is relatively quick-fading, and should be considered separately (see Section IV). The scenario used for all calculations in this paper is 20 GHz, 5° elevation angle, and the Washington D.C. area climate. The 5° elevation angle was selected as it produces especially strong contributions from all effects, and is probably the lower limit for useful communications (5° is being considered for extending coverage of fixed and mobile satellite systems). In Figure 1, the absorption by gas and clouds is calculated using a humid summertime scenario with moderate-heavy clouds. The surface water vapor density of 20 g/m^3 is used together with a Slobin height profile [8] that results in an integrated water vapor density of 4 cm, a value that is exceeded in Washington D.C about 10% of the time [5]. The cloud extends from 1 km above ground to 2 km above ground, with a uniform liquid water concentration of 1.0 g/m^3, giving a total liquid water content of 1.0 kg/m^2 . In statistics published by Salonen et al. [5], this level is exceeded approximately 5% of the time near Washington D.C.; it also corresponds to the total liquid water in Slobin's Case 8 cloud model [9], the lightest of the three 'Heavy Clouds'. The rain attenuation plotted is exceeded 2% of the year (98% availability) according to the Crane model [10] for climate region D2 (point rain rate = 1.5 mm/hr).

Figure 2 shows a comparison of the combined gaseous and cloud absorption for the scenario described above with radiometer measurements in Blacksburg, [11] and Wallops Island, [12] Virginia, both at 20.6 GHz, and with calculations at LaGuardia Airport, NY [9] at 18 GHz based on radiosonde measurements. This is an imprecise statistical comparison because, among other reasons, the Virginia measurements were for 1-2 month periods; nevertheless, the rough agreement observed is encouraging.

The modeling approach described here considers each effect individually, using accepted models where available. Each effect has a different mechanism of signal loss: rain produces Mie scattering of the wave, cloud water droplets produce absorption, water vapor and oxygen molecules undergo transitions that absorb energy, and turbulence refracts and diffracts the wave to produce scintillation. The different mechanisms require individual models to ensure that dependence on frequency, elevation angle, and weather parameters is correct for each effect.

The combination of these individual statistics requires the full joint distribution, for which sufficient information is not available. However, by describing the expected statistics of each effect by season or month instead of by year, we capture some of the nature of the correlation between effects. For example, weather-dependent models for gaseous absorption and tropospheric scintillation will both exhibit stronger effects in summer and weaker effects in winter.

The short-term correlations must also be considered. A cumulative distribution function (cdf) is developed for each effect, and the individual statistics are combined according to assumptions of either perfect statistical correlation ($\rho = 1.0$) or no statistical correlation (statistical independence, $\rho = 0.0$). Two random variables (RV's) which are perfectly correlated will experience extreme maxima simultaneously, and the same will be true of extreme minima. Accordingly, the cdf of the RV representing the combined process can be calculated simply by adding equiprobable values of the two constituent cdf's. For example, if the levels of gaseous absorption and cloud absorption not exceeded 90% of the summer are 6.8 dB and 1.2 dB, respectively, then under the assumption of perfect correlation, the level of combined absorption not exceeded 90% of the summer is 6.8 dB + 1.2 dB, or 8.0 dB.

The sum of two independent RV's is obtained by convolving the two probability density functions (pdf's) to obtain the pdf of the combined process, or by convolving one cdf with one pdf to obtain the cdf of the combined process.

We will describe two modeling approaches in this paper: summer statistics, for which example results of combined effects models will be presented; and month-by-month statistics. The latter approach can also be used to produce seasonal and annual statistics; we point out in the following sections some of the components of such an approach. The following sections consider each effect individually in terms of a monthly model, a summertime model, and preliminary approaches for combining with other effects. PMOD (Propagation MODel), the software propagation analysis tool developed by Stanford Telecom, will incorporate the models discussed in this paper

II. Gaseous Absorption

Water vapor and oxygen are the two gasses that contribute significant attenuation in the microwave region [13]. In the Ka band, oxygen absorption is typically an order of magnitude (in dB) smaller than water vapor absorption, and the fluctuations in water vapor absorption dominate the gaseous absorption statistics in this band. In addition, the variation in water vapor absorption depends principally on the total water vapor in the path. These last two points are demonstrated in Figure 3.

Figure 3 depicts the predictors of gaseous (both water vapor and oxygen) absorption. The sample points were calculated by integrating the Liebe model for specific absorption [13] over radiosonde profiles of temperature, pressure, and humidity taken during the summer of 1994 (June through mid-September) in the Washington D.C. area. Temperature (Figure 3a) is a poor predictor; surface humidity (Figure 3b) is fairly good but flawed, as will be discussed below; but integrated water vapor (Figure 3c) is an excellent predictor. The correlation between integrated water vapor and *water vapor* absorption alone has been shown by Salonen et al. [4] to be even better. (The non-zero y-intercept in Figure 3c represents the oxygen absorption.) Thus, we may reduce the height profiles of three parameters to the integrated value of a single parameter, water vapor, and incur very little error in the calculation of absorption. Moreover, note also the linearity of the relation between integrated water vapor and gaseous absorption. This allows the statistics of

integrated water vapor to be mapped directly to statistics of gaseous absorption, which greatly simplifies computer calculations of absorption statistics.

This characteristic has led to a preliminary computer model (included in PMOD) which implements long-term surface weather data. The program stores, for each month, the mean surface temperature and a tabulated cdf of the surface humidity. The user may specify the desired non-exceedance probability (analogous to availability) and the program takes the corresponding level of surface water vapor, the mean surface temperature, and the standard surface pressure, and integrates the Liebe specific absorption model over the resultant height profiles. This approach was tested by comparing with the accumulated statistics resulting from integrations of the Liebe model over the Slobin profiles at each hourly measured set of surface temperature/pressure/humidity over 10 years, and the cdf's were in very good agreement (see Figure 4).

The model, however, is not complete, because surface water vapor does not adequately characterize the water vapor over the radio path (for systems with high elevation angles, however, the error may be small). See Figure 5, which presents a cdf of gaseous absorption based on integrated water vapor, and a second cdf based on surface water vapor density and the Slobin average height profiles. This figure derives from the same data shown in Figure 1. The average profiles produce accurate estimates of the mean absorption, but miss many of the higher values of absorption, which are most important to link design. The data represented by the solid line will be used as the summertime absorption statistics in combined effects modeling in the following sections.

In future work, we will derive from radiosonde data the long-term statistics of integrated water vapor by month, which will provide for an improved mapping to monthly absorption statistics. An alternative source of this information is available in Salonen et al. [5], based on analysis of global ECMWF (European Center for Medium Range Weather Forecasts) data.

III. Cloud Absorption

Absorption by clouds is the most difficult to model statistically at the current time. The relevant cloud parameter is the total liquid water content, which is required in the form of a cdf, preferably by month or season. The importance of cloud absorption is enhanced because it occurs in conjunction with all other effects considered here. Rain occurs in the presence of clouds. Tropospheric scintillation is produced by turbulence, which is often associated with clouds (observations of the connection between scintillation and clouds were reported by Cox et al. [14], among others). Finally, gaseous absorption increases with humidity, which is also associated with increased water content in the cloud (higher absolute humidity makes more water vapor available for condensation into cloud liquid water).

Salonen et al. [15] have developed a model for cloud liquid water content that uses measured vertical weather profiles to estimate the existence, extent, and density of clouds. They have also published extensive statistics for Europe and the globe on cloud liquid

water [5]. These statistics are based on one full year of data and are not broken into season or month. In our estimates of summer statistics we have applied a scaled (in frequency and elevation angle) version of the full-year cloud absorption statistics reported for Finland (which under-estimates the summer absorption statistics). The results compare well with Slobin's models of typical cloud types [9]. Figure 6 illustrates the combination of gas and cloud absorption into a total absorption amount using two reasonable extremes: total correlation and total independence (negative correlation is not expected so it is not included). The two estimates of combined absorption differ by up to 2 dB at high percentages. Salonen et al. [7] have compared results based on these two extremes with the true combined statistics in Europe and found better results with the equiprobable assumption in most of northern Europe, and better results with the independent assumption in Mediterranean climates.

In order to create monthly and seasonal statistics, we plan to apply the Salonen cloud detection and liquid water estimation model to local radiosonde data.

IV. Scintillation

Tropospheric scintillation is produced by turbulence in humid air, accordingly, both humidity and turbulence are necessary for strong scintillation. The model developed by Karasawa et al. [16] uses two levels of statistics to describe these dependencies. The first is a short-term (valid over 10-60 min) Gaussian distribution of the fade level, $f_1(x)$, with zero mean and a variable standard deviation (scintillation intensity) described statistically by the second tier. The second tier is a Gamma distribution, $f_2(\sigma)$, applied to month-long periods. A function is given for mapping mean temperature and humidity for the month into the mean of the Gamma distribution of intensity, σ_m. The cdf of the fade level is computed by:

$$P(x < X) = \int_{-\infty}^{X} \int_{0}^{\infty} f_1(z|\sigma) f_2(\sigma) d\sigma dz . \qquad (1)$$

One approach to combining scintillation and absorption is to assume independence over the course of the month, with the average levels for each month related through the mutual dependence on temperature and humidity. In this case, a convolution of fade level statistics gives the combined statistics. However, there is reason to expect greater correlation and higher scintillation intensity during particularly humid afternoons, for example. In fact, the correlation exists over any time period, it merely decreases as the period shortens. This has been observed, and the correlation has been quantified by Vogel et al. [17] over a range of time periods, down to 43% correlation over one hour periods. Therefore, an upper bound to the combined statistics would be an equiprobable relationship between gaseous absorption and scintillation intensity. Note that the appropriate relationship is *not* between absorption and scintillation fade level. During scintillation, the signal level rapidly fluctuates about a much more slowly fluctuating mean, so all values of the short-term scintillation distribution, positive and negative, occur during periods of extreme scintillation

The cdf of the combined effect in this case is obtained by integrating over the Karasawa relation in Eq. (1) with the modification that the mean of f_l is not zero, but rather is equal to the level of absorption equiprobable with the standard deviation (intensity) of the short-term statistics. The equiprobable mapping is thus between the cdf of absorption and the cdf of scintillation intensity, the latter described by the Gamma distribution.

Figure 7 shows the expected summer statistics with rain effects excluded. The equiprobable (worst-case) combination of gas and clouds is presented without scintillation for comparison, and combined with scintillation according to the independent and correlated assumptions. The mean scintillation intensity over the summer is taken as 0.8 dB.

V. Rain

The Crane rain model [10] applied to the D2 climate region is combined with secondary effects in two ways in Figure 8. In the first, the mean gaseous absorption is added to the rain attenuation distribution. This is a typical propagation analysis, but is applied here using the summer mean gaseous absorption rather than the annual. The second method is an independent combination of the rain statistics with the worst-case non-rain statistics. The non-rain curve, also shown in the figure, assumes correlation between gaseous absorption, cloud absorption, and tropospheric scintillation intensity. The gaseous absorption and scintillation data, discussed above, are based on summer weather, while the cloud and rain statistics are annual predictions. For this particular scenario and set of assumptions, the curves representing a basic mean absorption and a full combined statistics approach converge somewhere slightly above 99% availability, where rain attenuation asserts its dominance over the other effects. This estimate of combined effects statistics is rather optimistic, however, because rain attenuation is assumed independent of other effects. By correlating rain with the other effects (cloud absorption, in particular, is correlated), predicted availability will degrade.

A monthly model for rain statistics in the Washington area is possible through the rain rate statistics reported by Goldhirsh and Gebo[18] over 8 years at 10 sites. This will be incorporated in future work.

VI. Conclusions

The seasonal dependence of all of the propagation effects discussed here: gas and cloud absorption, scintillation, and rain attenuation, is very strong for most climates, and generally all effects are enhanced in the summer (for the northern hemisphere). The correlation between effects is variable, but bounds may be produced on the combined effects through bounds on the likely correlation. This work only begins to address the possible correlations. The combined effects estimates presented here, by building up from gaseous absorption to gas and clouds, etc., emphasized the non-rain propagation effects, which have not been considered statistically in the past. However, since rain is often dominant, estimates should also be made starting from the rain statistics and correlating various effects with rain. Useful information for this effort would include weather statistics (humidity and cloud water content) conditioned on the existence and possibly the

intensity of rain. Future work includes developing monthly conditional statistics of integrated water vapor and cloud liquid water, investigating cloud modeling further, and comparing ACTS beacon and radiometer data with models utilizing ACTS weather data.

VII. References

[1] G. Brussaard and D. V. Rogers, "Propagation considerations in satellite communication systems," *Proc. IEEE*, vol. 78, pg. 1275-1281, July 1990.

[2] J. E. Allnut and D. V. Rogers, "Low-fade-margin systems: propagation considerations and implementation approaches," *Proc. Int. Conf. Antennas Propagat.*, IEE Conf. Publ. 301, 1989, pg. 6-9.

[3] J. P. V. Poiares Baptista and G. Brussaard, "Propagation predictions for low-elevation, low-availability satellite systems," *El. Lett.*, vol. 25, no. 20., pg. 1391-1393, Sept. 1989

[4] E. Salonen et al., Study of propagation phenomena for low availabilities, Final Report for ESA under ESTEC contract 8025/88/NL/PR, 316 pg., Nov. 1990.

[5] E. Salonen et al., Study of improved propagation predictions, 1994, Final Report for ESA under ESTEC contract 9455/91/NL/LC(SC), Dec. 1994.

[6] E. Salonen et al., "Modeling and calculation of atmospheric attenuation for low-fade-margin communications," *ESA Journal*, vol. 16, no. 3, pg. 299-317, 1992.

[7] E. Salonen, "Prediction models of atmospheric gases and clouds for slant path attenuation," *Olympus Utilisation Conference*, Sevilla, pg. 615-622, April 1993.

[8] S. D. Slobin, Microwave noise temperature and attenuation of clouds at frequencies below 50 GHz, JPL Publ. 81-46, July, 1981.

[9] S. D. Slobin, "Microwave noise temperature and attenuation of clouds: Statistics of these effects at various sites in the United States, Alaska, Hawaii," *Rad. Sci.*, vol. 17, no. 6, pg. 1443-1454, Nov.-Dec. 1982.

[10] R. K. Crane, "Prediction of attenuation by rain," *IEEE Trans. Comm.*, vol. COM-28, no. 9, Sept. 1980.

[11] J. B. Snider et al., "Comparison of Olympus beacon and radiometric attenuation measurements at Blacksburg, Virginia," *Proc. NASA Propagat. Exper. Mtg., (NAPEX XV)*, June 1991.

[12] J. B. Snider et al., "Observations of attenuation at 20.6, 31.65, and 90.0 GHz - Preliminary results from Wallops Island, VA," *Proc. NASA Propagat. Exper. Mtg., (NAPEX XIII)*, June 1989.

[13] H. J. Liebe, "An updated model for millimeter-wave propagation in moist air," *Rad. Sci.*, vol. 20, no. 5, pg. 1069-1089, Sept-Oct. 1985.

[14] D. C. Cox, H. W. Arnold, and H. H. Hoffman, "Observations of cloud-produced amplitude scintillation on 19- and 28- GHz earth-space paths," *Rad. Sci.* vol. 16, pg. 885-907, Sept.-Oct. 1981.

[15] E. Salonen and S. Uppala, "New prediction method of cloud attenuation," *El. Lett.*, vol. 27, no. 12, pg. 1106-1108, June 1991.

[16] Y. Karasawa, M. Yamada, and J. E. Allnut, "A new prediction method for tropospheric scintillation on earth-space paths," *IEEE Trans. Antennas Propagat.*, vol. 36, pg. 1608-1614, Nov. 1988.

[17] W. J. Vogel, G. W. Torrence, and J. E. Allnut, "Scintillation fading on a low elevation angle satellite path: Assessing the Austin experiment at 11.2 GHz," *Proc. Int. Conf. Antennas Propagat.*, March 1993.

[18] J. Goldhirsh and N. E. Gebo, "Slant path attenuation statistics at 20 GHz and 30 GHz from an eight year data base of rain rates obtained from the mid-Atlantic coast rain gauge network," *ACTS Propagat. Studies Workshop (APSW VI)*, pg. 271-281, Nov. 1994.

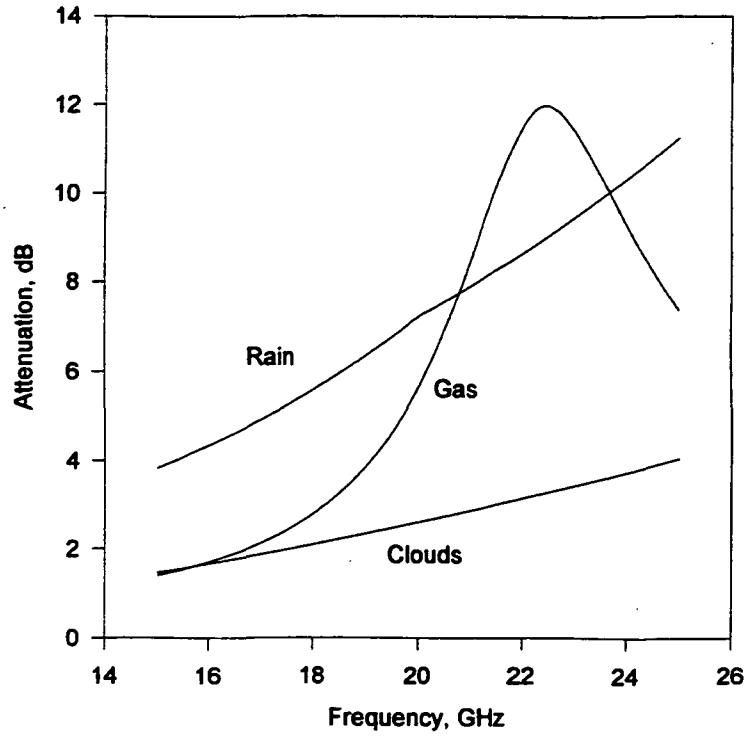

Figure 1. Individual propagation effects

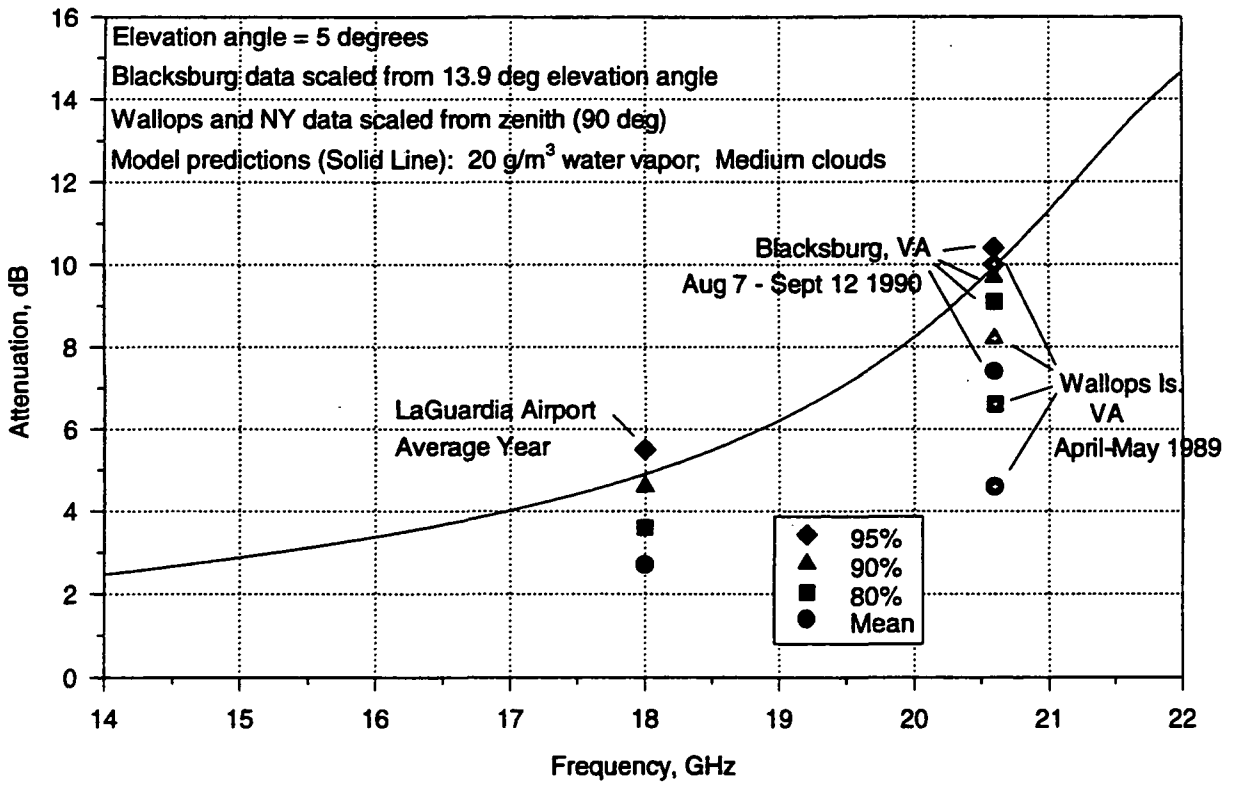

Figure 2. Predictions of absorption by gas and clouds with Liebe model, compared to radiometer measurements in Virginia and weather-based calculations in NY.

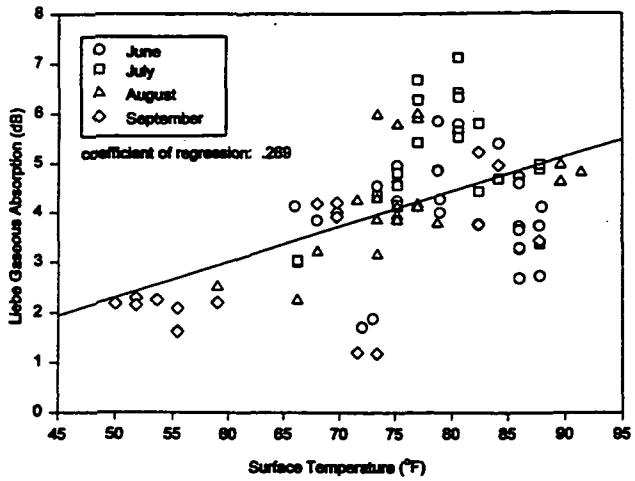

Figure 3a. Radiosonde-based Liebe gaseous absorption vs. surface temperature

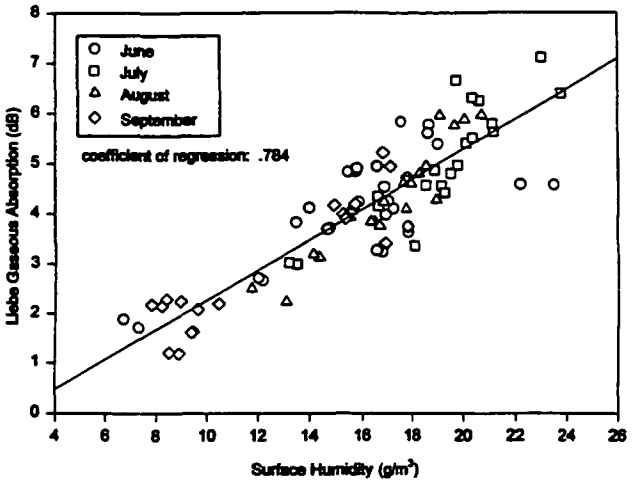

Figure 3b. Radiosonde-based Liebe gaseous absorption vs. surface humidity

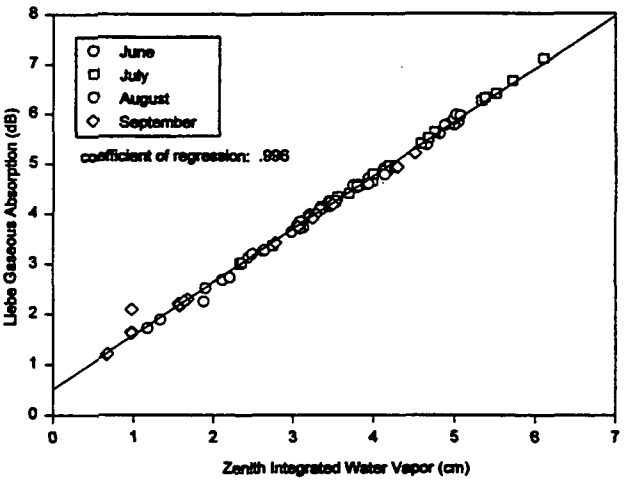

Figure 3c. Radiosonde-based Liebe gaseous absorption vs. integrated water vapor

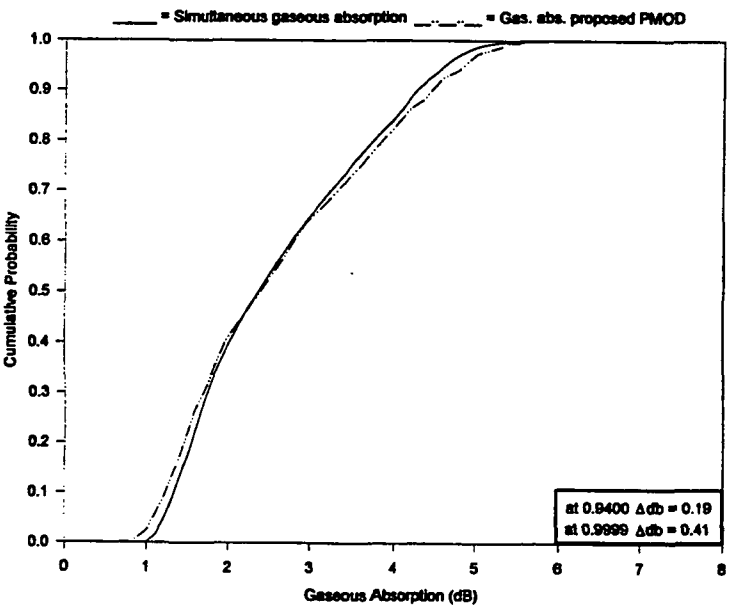

Figure 4. Annual gaseous absorption cdf's based on 1984-1994 surface observations: test of proposed model

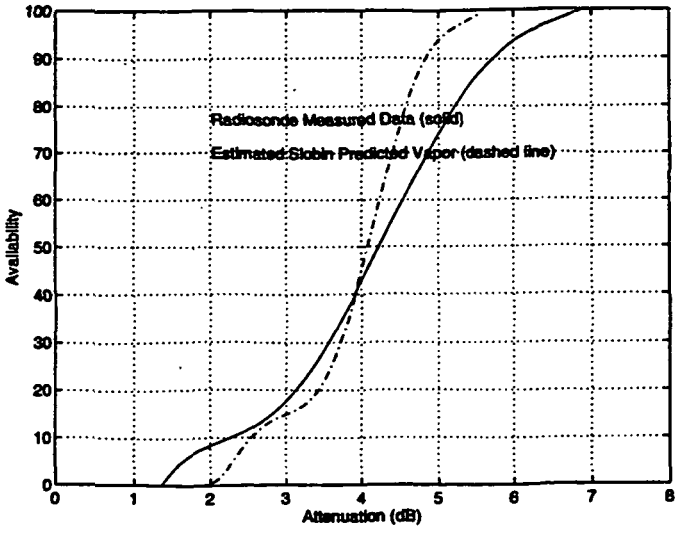

Figure 5. Error in surface-based gaseous absorption model

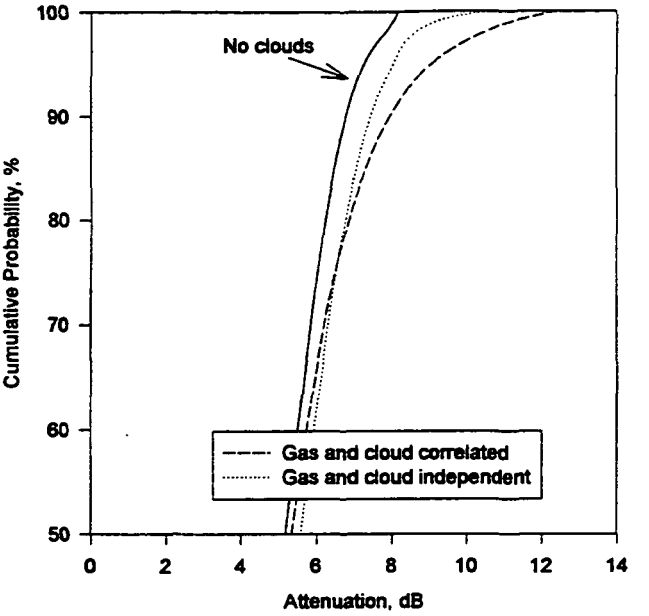

Figure 6. Absorption by gas and clouds; gaseous absorption based on summer radiosonde data, cloud absorption from Salonen and Uppala [15] (annual)

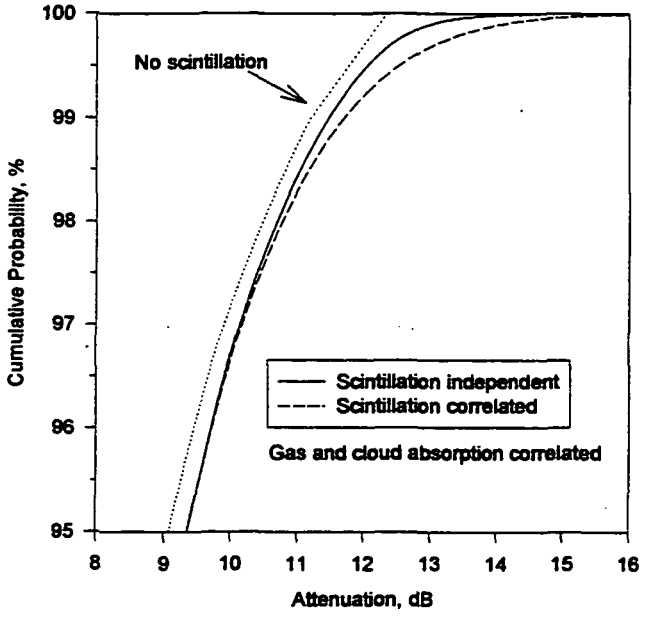

Figure 7. Attenuation by gas, clouds, and scintillation; summer statistics used for gaseous absorption and scintillation, annual for clouds

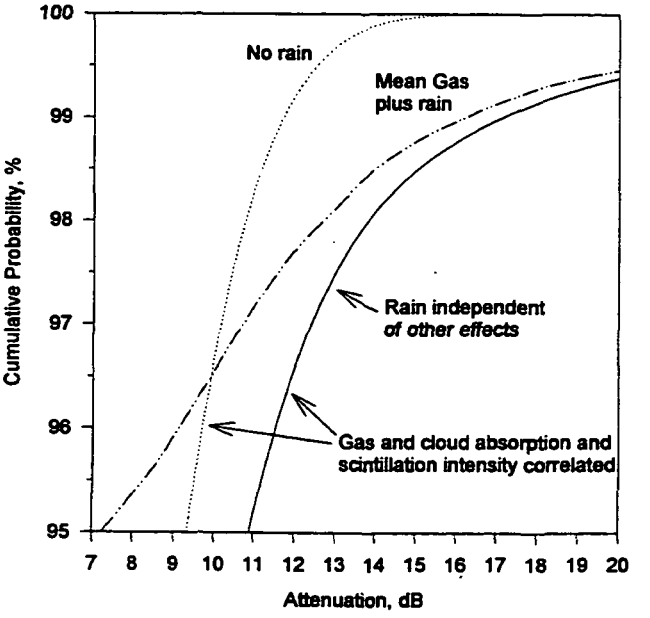

Figure 8. Attenuation by rain, gas, clouds, and scintillation; summer statistics used for gas and scintillation, annual for rain and clouds